Solar Wind-Magnetosphere Coupling: A Global Perspective of Substorm Onset

Miles Bengtson, Katariina Nykyri

Abstract. We present a case study of the 25 December 2015 substorm which occurred between 08:15 and 08:45 Universal Time. During this interval, fast particle flows and field geometry consistent with magnetic reconnection were detected in the mid-tail region. An ejected plasmoid was observed by the lunar-orbiting Acceleration, Reconnection, Turbulence and Electrodynamics of Moon's Interaction with the Sun (ARTEMIS) probes and a corresponding dipolarization signature was observed by the Time History of Events and Macroscale Interactions During Substorms (THEMIS) probes earthward of the reconnection site, which was determined to be approximately -33 R_E. Ground signatures indicative of substorm activity were also observed by the THEMIS ground-based observatories during this interval. Immediately prior to the substorm, none of the solar-wind monitoring missions (OMNI, Geotail, ACE) observed a significant southward B_z which could have initiated the event. The Magnetospheric Multiscale (MMS) probes, which were in the dayside magnetosheath, detected a strong pulse in B_z, with a minimum near -35 nT, at 08:00 UT, consistent with the time delay required for propagation from the magnetosheath to the mid-tail. We analyze and discuss these pulsations and propose that this strong southward component of B_z in the magnetosheath is associated with the substorm trigger. We simulate the entire magnetosphere in maximum detail for this event using the Space Weather Modeling Framework/Block Adaptive Tree Solar-wind Roe Upwind Scheme (SWMF/BATS-R-US) model from NASA's Community Coordinated Modeling Center (CCMC) with a special, high-resolution grid. The results of this work will be highly relevant to future solar wind observation missions, global-scale magnetohydrodynamic (MHD) models, and the ongoing effort to understand how processes at lunar distances in the tail couple to the rest of the near-Earth space environment.

1. Introduction

Substorms occur when magnetic energy stored in the Earth's magnetotail is suddenly released into particle thermal or kinetic energy and the global magnetic field becomes reconfigured [*Akasofu*, 1964; *Axford*, 1999]. Signatures associated with substorms include intensification and expansion of the auroral arc, an increase in the ionospheric electroject, particle injections into the ionosphere and magnetosphere, and a plasmoid ejected tailward. The energy released in the substorm originates in the coupling of the solar wind with the magnetosphere [*Dungey*, 1961; *Baker et al.*, 1997]. The coupling is particularly strong during prolonged periods of southward interplanetary magnetic field (IMF) [*Nishida*, 1983; *Rostoker et al.*, 1980; *Caan et al.*, 1977]. This ensures that the field lines of the solar wind are directed anti-parallel to the closed dipole field lines of the Earth, allowing reconnection to occur on the dayside. The newly opened field lines then propagate tailward, storing energy in the form of magnetic flux in the tail regions (the growth phase of the substorm). *Borovsky et al.* [1993] report that about 1500 substorms occur per year, with about half occurring in periodic intervals having an average time between substorm onsets of 2.75 hours. Other studies have shown an occurrence rate of substorm related phenomena of one event per 3.9 hours [*Fu et al.*, 2012].

Substorms are closely linked to a number of ionospheric phenomena which can be detected from the ground. These phenomena include sudden intensification and expansion of the aurora [*Akasofu*, 1964], a sharp increase in the the auroral electrojet (AE) index, and magnetic field pulsations associated with substorm-generated ionospheric currents [*Saito*, 1969]. Fluctuations in this current system are detected as pulsations in the ground magnetic field in the 40-150 sec range, known as Pi2 pulsations [*Saito*, 1969].

Until recently, the trigger mechanism for substorm onset was under debate. The two main models included the current sheet disruption model [*Lui*, 1996] and the Near-Earth Neutral Line (NENL) model [*McPherron et al.*, 1973; *Baker et al.*, 1996]. The disruption model proposes that substorm onset is triggered by a thinning of the current sheet in which whistler waves are produced by ion-electron interactions at around 10 R_E. These waves cause the plasma sheet to act resistively, thereby disrupting the cross-tail current and diverting it through the ionosphere. This model asserts a substorm onset location much closer to the earth (10 R_E) than the NENL model. According to the Near-Earth Neutral Line model, field lines which have become stretched by the accumulation of magnetic flux in the tail reconnect at a downtail distance of 20 - 40 R_E, thereby triggering the release of energy. Plasma in the plasma sheet boundary layer above or below the X-line region flows toward the reconnection site. The plasma in the neutral sheet near the reconnection site is heated and accelerated, flowing earthward on the earthward side of the reconnection site and tailward on the tailward side. Subsequently, a dipolarization front, or rapid increase in the north-south magnetic field component (B_z) [*Runov et al.*, 2009], propagates earthward from the reconnection site. The earthward flows interact with the near-Earth currents, creating a circuit through the ionosphere known as a substorm current wedge (SCW) [*Atkinson*, 1967]. The SCW couples the magnetospheric processes to the ionosphere, producing auroral intensifications and Pi2 pulsations. A plasmoid, or magnetic loop containing heated, confined plasma,

[1]Embry-Riddle Aeronautical University, Daytona Beach, Florida, USA

0148-0227/17/$9.00

is launched tailward along the neutral sheet toward the Distant Neutral Line (DNL) in what is often termed a nightside flux transfer event (NFTE) [*Richardson and Cowley*, 1985; *Sergeev et al.*, 1992; *Ieda et al.*, 1998]. The energy contained within the plasmoid eventually returns to the solar wind.

The goal of the Time History of Events and Macroscale Interactions During Substorms (THEMIS) mission [*Angelopoulos*, 2008] was to determine which of these two models is supported by evidence and to establish a timeline of substorm events for different regions of the magnetosphere. The initial mission consisted of five identical probes in orbits that aligned in major conjunctions along the Earth-Sun line every four days, allowing simultaneous multipoint measurements to be taken throughout the expected substorm initiation region of -10 R_E to -30 R_E. Additionally, a dense array of magnetometer and all-sky imager stations were deployed across Canada and Alaska to establish timing of substorm ground phenomena. THEMIS observations have recently established that substorms are triggered by reconnection which occurs at around 20 R_E downtail [*Angelopoulos et al.*, 2008; *Liu et al.*, 2009; *Gabrielse et al.*, 2009; *Pu et al.*, 2010], as predicted by the NENL model. Further, observations have shown there is a propagation time of approximately 2-4 minutes between reconnection and auroral signatures and Pi2 pulsations being observed on the ground.

In this paper, we present observations of a substorm on 25 December 2015 in which a dipolarization front and plasmoid were observed in the near and far magnetotail, respectively. This study differs from previous timing case studies, however, in that we consider the dayside events in detail along with the tail observations, thus establishing a timeline of events which includes disturbances in the solar wind, dayside magnetosheath, near-Earth and far-tail regions. A fortuitous alignment of several independent spacecraft missions (THEMIS/ARTEMIS, MMS, and Geotail) near the Earth-Sun line allows a comprehensive analysis of the global magnetosphere during a substorm event. Considering that the ARTEMIS probes cross the tail region during only several days per month, it is unique to have multipoint measurements spanning nearly 80 R_E from upstream of the bowshock to the far-tail. In Section 3.2, we discuss observations and timing analysis from the THEMIS and ARTEMIS missions. We discuss in Section 3 the coupling of the solar-wind and dayside magnetosheath physics with the substorm processes in the tail using data from Geotail and Magnetospheric Multiscale (MMS). Finally, we present results from global-scale MHD simulations in Section 4.

2. Methodology

In this study, we use data from the THEMIS, ARTEMIS, MMS, and Geotail missions. The two ARTEMIS probes were originally part of the five spacecraft THEMIS mission, launched in 2007, to study the substorm onset mechanism in the near-Earth tail [*Angelopoulos*, 2008]. In 2010, THEMIS probes B and C (henceforth referred to as P1 and P2, respectively) were transferred to lunar orbit thus commencing the ARTEMIS mission, while THEMIS A, D, and E (henceforth referred to as P5, P3, and P4, respectively) remain in the near-Earth magnetosphere [*Angelopoulos*, 2011]. During approximately three days per month, the ARTEMIS spacecraft cross the magnetotail at ∼60 R_E. We use particle data from the Electrostatic Analyzer (ESA, 3 s resolution, 10 eV - 28 keV) [*McFadden et al.*, 2008] and Solid State Telescope (SST, 3 s, 28 keV - 2 MeV) [*Angelopoulos*, 2008] and field data from the Fluxgate Magnetometer (FGM, 1/8 s) [*Auster et al.*, 2009]. The four MMS spacecraft were located on the dayside during this event. We use particle data from the Fast Plasma Investigation (FPI) (4.5 s, 10 eV - 30 keV) [*Pollock et al.*, 2016] and field data from the Fluxgate Magnetometer (1/16 s) [*Russell et al.*, 2014; *Torbert et al.*, 2016]. The Geotail spacecraft was located in the solar wind during the interval of interest. We use field data obtained by the Magnetic Field Experiment (MGF, 1/16 s) [*Kokubun et al.*, 1994] and particle data from the Low Energy Particle experiment (LEP, 12 s) [*Mukai et al.*, 1994]. Table 1 and Figure 1 provide the location of each spacecraft at 0815 UT on 25 December 2015 along with field line traces from the Tyganenko 89 model [*Tsyganenko*, 1989]. Data throughout is presented in Geocentric Solar Magnetospheric (GSM) coordinates.

We model this event using a custom, high-resolution grid within the Space Weather Modeling Framework (SWMF)/Block Adaptive Tree Solar-wind Roe Upwind Scheme (BATS-R-US) model hosted by NASA's Community Coordinated Modeling Center (CCMC) [*Tóth et al.*, 2005, 2012]. This code solves the magnetohydrodynamic (MHD) equations in a block-adaptive mesh which can be applied to simulate the coupling of the solar wind with the global magnetosphere. Model inputs include the date and time of the event to accurately model the Earth's field configuration and the solar wind field and plasma parameters at the upstream model boundary.

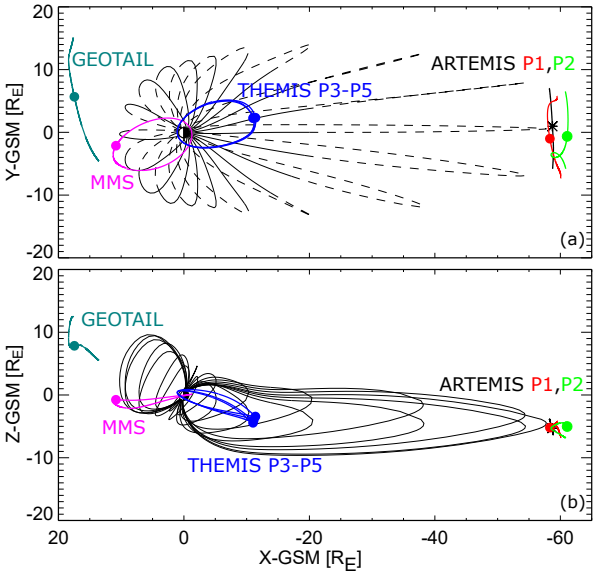

Figure 1. Positions of ARTEMIS, THEMIS, MMS, and Geotail spacecraft in the (a) XY plane and (b) XZ plane at 0815 UT on 25 December 2015. The black lines are field lines as traced with the Tsyganenko 89 model. In panel (a), the solid field lines are above the Z = 0 plane, whereas the dashed field lines are below it.

Table 1. Spacecraft locations at 0815 UT.

Spacecraft	X_{GSM} [R_E]	Y_{GSM} [R_E]	Z_{GSM} [R_E]
ARTEMIS P1	-58.3	-1.0	-5.2
ARTEMIS P2	-61.1	-0.64	-5.0
THEMIS P5	-11.4	2.3	-3.4
THEMIS P3	-11.0	2.3	-4.4
THEMIS P4	-11.1	2.3	-4.0
MMS1[a]	10.8	-2.1	-0.76
GEOTAIL	17.5	5.7	7.8

[a]MMS probes were within a 30 km formation.

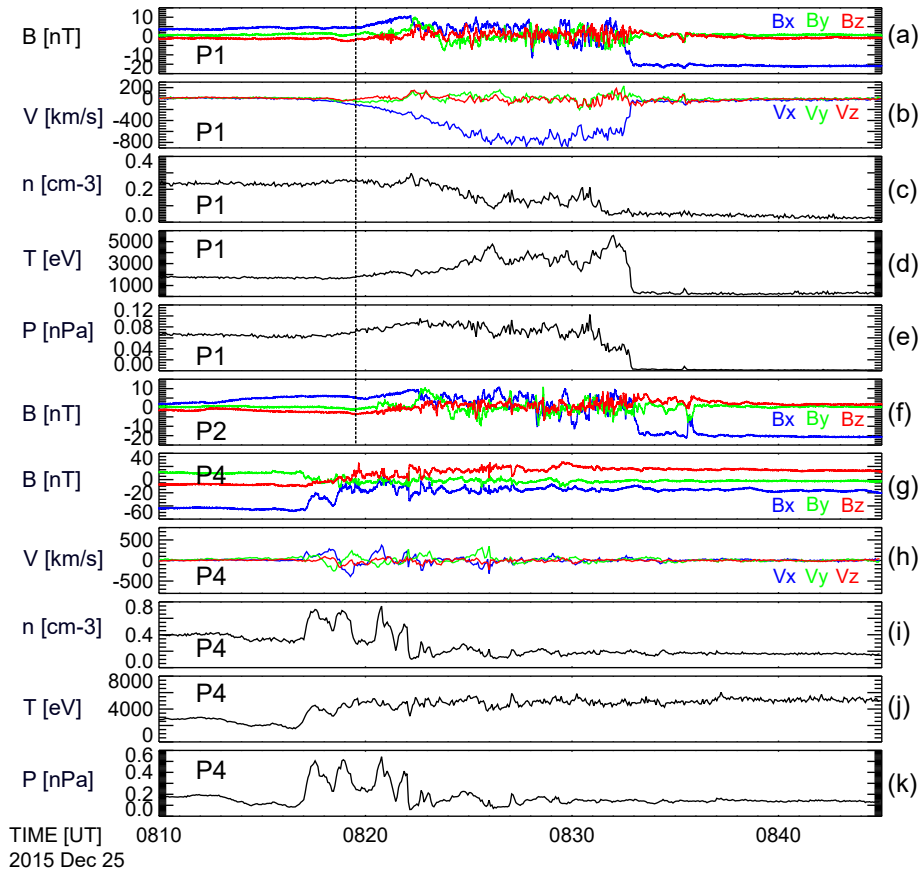

Figure 2. Magnetic field, ion velocity, density, temperature, and pressure for (a-e) ARTEMIS P1, (f) magnetic field for P2, and Magnetic field, ion velocity, density, temperature, and pressure(g-k) for THEMIS P4. The vertical line denotes 08:19.

3. Results and Discussion

3.1. Overview

During the 25 December 2015 substorm, the THEMIS, ARTEMIS, MMS, and Geotail spacecraft were all aligned approximately parallel to the Earth-Sun line. Table 1 provides the position of each spacecraft around the time of substorm onset. Figure 1 shows the location of each spacecraft at this time, along with orbit traces for the entire day. Note that the black lines in each panel are magnetic field lines, traced using the Tyganenko 89 model [*Tsyganenko*, 1989].

3.2. Magnetotail Observations

Figure 2 shows an overview of field and plasma data from the ARTEMIS and THEMIS probes. From 08:17:00 to 08:25:00 UT, the tailward particle velocities (negative V_x) at P1 slowly ramp up from near 0 to a maximum value of ∼800 km/sec which persists until 08:33:00. Tailward flow speeds between 500 and 800 km/sec are consistent with reconnection outflow jets reported in case studies of the tail at mid to near-lunar distances [*Øieroset et al.*, 2000; *Oka et al.*, 2011]. At 08:19:50, B_x increased from 5 to 10 nT, then began to fluctuate between positive and negative values. At the end of the event interval, B_x turned to -15 nT. P2, which was 2.8 R_E further downtail from P1, observed a nearly identical signature, though the particle flows began to increase at 08:19:20 and the magnetic structures arrived at 08:20:10. On the near-Earth side (∼-11.0 R_E), P3-P5 observe a dipolarization front in the magnetic field at 08:17:05, in which the B_x component changes from having a negative value to zero while the B_z component goes from zero to positive [*Runov et al.*, 2011]. Only data from P4 is shown, as it is representative of that from the other near-Earth probes. Coincident with the dipolarization front, the earthward flow speed, plasma temperature, and plasma density increase sharply. We interpret these observations as outflows and field signatures associated with reconnection which occurred prior to this time in the mid-tail. A north-then-south turning of the magnetic field, as was observed by P1 and P2, is a typical signature of a passing plasmoid in the tail. To confirm that the observed structure is indeed a plasmoid, the pressure enhancement inside the plasmoid should be at least 10% of the baseline value, as discussed by *Ieda et al.* [1998]. The pressure inside the structure has a maximum near >0.09 nPa, whereas the baseline value before the event was ∼0.065 nPa, indicating a total pressure enhancement of ∼38%. Therefore, we conclude that this structure is indeed a passing plasmoid ejected tailward during the reconnection. The observed plasmoid matches typical parameters determined in statistical studies of plasmoids using Geotail observations. The ion temperature inside the structure of between 3 and 5 keV is similar to that reported by *Ieda et al.* [1998], as is the ion to electron temperature ratio of ∼16. P2 was 2.8 R_E further downtail from P1 and observed the same particle flows 111 sec after P1. This time delay indicates that the plasmoid structure was moving at a velocity of ∼160 km/sec tailward. Assuming the plasmoid is neither accelerating nor expanding, the overall length can be estimated by considering the duration over which the flow channel was observed. Considering that the flows persisted for 16 minutes, this gives an estimate for the plasmoid length as ∼20 R_E. *Nagai et al.* [1997] reported a median flow duration for plasmoids in the region from -80 to -100

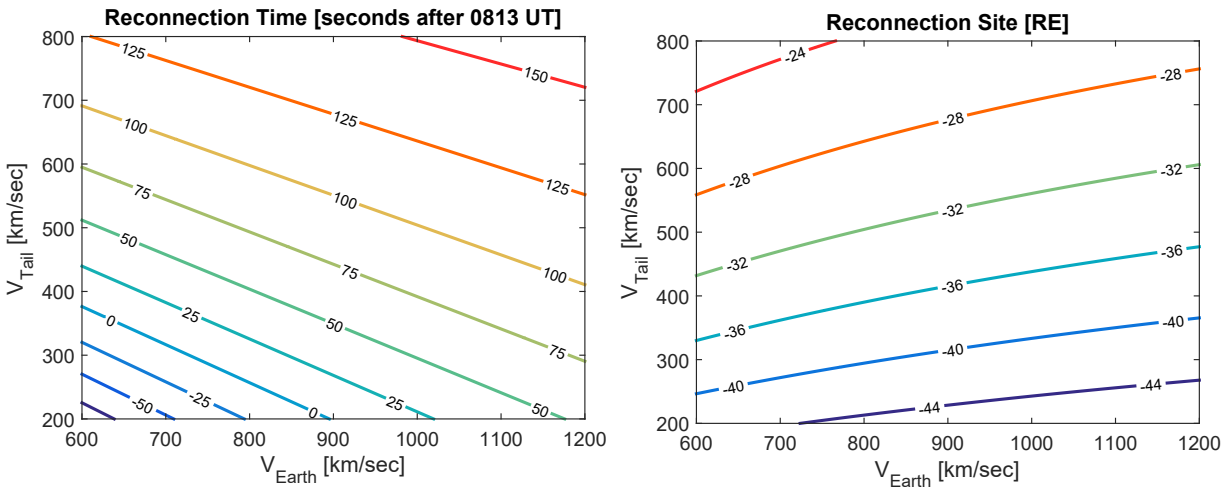

Figure 3. (left) Reconnection onset time and (right) X-line location dependence on propagation speeds.

R_E to be 17 minutes, comparable to the expansion phase of substorms. Previous estimates for plasmoid length have ranged from 17 to 35 R_E [*Slavin et al.*, 1984; *Moldwin and Hughes*, 1992]. The oppositely directed flows at P1-P2 and P3-P5 indicate that the reconnection X-line was located in the mid-tail region between these observation points. Given the positions of two probes on either side of the reconnection location and the times at which substorm phenomena were first detected at each location, we can determine the time and location at which reconnection occurred. Unlike previous work which assumes a constant propagation speed on both sides of the reconnection site [*Angelopoulos et al.*, 2008; *Liu et al.*, 2009; *Mende et al.*, 2009], we use here the equations presented by *Liu et al.* [2011] which allow for different tailward and earthward propagation speeds. Whereas assuming one propagation speed is reasonable over short distances, this assumption is invalid considering the ¿45 R_E probe separation considered in this event. We do assume that the propagation speed is constant on either side of the reconnection site and that the propagation is entirely in the X-direction. These equations are as follows:

$$X_E - X_R = V_E \left(T_E - T_R\right), \tag{1}$$

$$X_R - X_T = V_T \left(T_T - T_R\right), \tag{2}$$

where X_R and T_R are the location and time of the reconnection site, respectively, V_E and V_T are the earthward and tailward magnetosonic speeds, X_E and X_T are the respective probe positions, and T_E and T_T are the times at which the signatures were observed in each location. The inferred reconnection position and onset time are heavily dependent on the magnetosonic speeds used in the calculation. Figure 3 shows the reconnection site and time with varying earthward and tailward magnetosonic speeds. We consider the dipolarization field at P3 (08:17:05) as the earthward observation time and the magnetic structure at P1 as the tailward observation time (08:19:50). Assuming an earthward propagation speed of 800-1000 km/sec and a tailward propagation speed of 400-600 km/sec, the reconnection site is determined to be 33.2 ± 2.4 R_E. The reconnection onset time for this range is 08:13:49 - 08:14:59. Ground-based observations from the THEMIS all-sky imager and magnetometer networks show magnetic pulsations in the Pi2 range (40-150 sec) [*Saito*, 1969] beginning at 08:17:33. This is in agreement with the previously determined reconnection time, considering a typical time delay between reconnection and ground onset of 2-4 minutes. The magnetometer data is provided and discussed in more detail in the Appendix.

3.3. Dayside Observations

The Geotail spacecraft was located in the solar wind during the 25 December 2015 substorm, just outside of the bowshock. Therefore, the plasma parameters and magnetic field observed by Geotail, shown in Figure 4, are indicative of those acting upon the magnetosphere. In addition, field and plasma parameters from the OMNI virtual spacecraft and ACE (propagated to the bowshock nose) are provided and are in good agreement with the Geotail observations. Geotail observes a large-scale oscillation of the IMF from 07:00 to 09:00 on 25 December 2015. The IMF is southward with B_z values near -4 nT from 07:00 to 07:40. From 07:40 to 07:51, B_z has small negative values ($\sim$ -2 nT) and turns northward at 07:51:10 (denoted by the vertical line in the Figure).

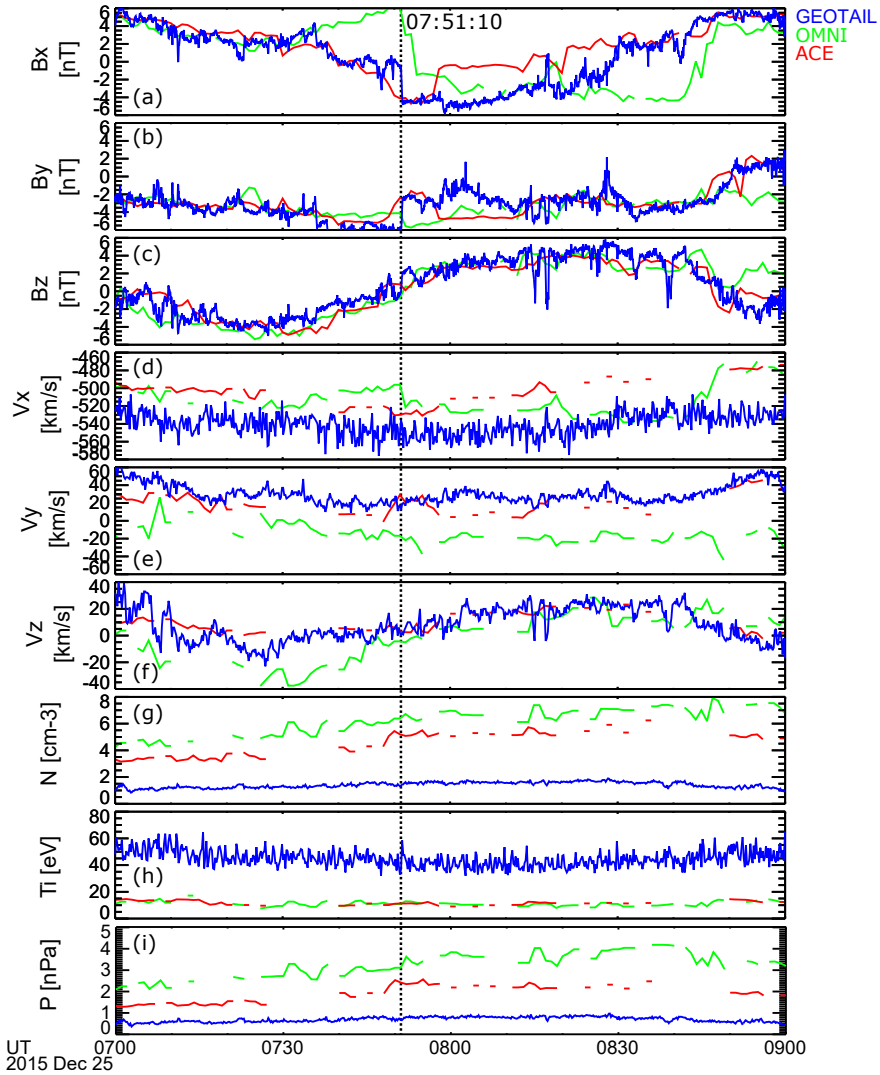

Figure 4. Magnetic field components (a)-(c), velocity components (d)-(f), ion density (g), ion temperature (h), and pressure (i) in the solar wind prior to the substorm observed by Geotail, ACE (propagated to bow shock), and OMNI.

During the interval of interest, the MMS probes were located in the dayside magnetosheath, just outside the magnetopause boundary (see Figure 1 and Table 1). Figure 5 shows magnetic field and plasma data for MMS1 from 07:50 to 08:30. In the minutes prior to the substorm onset in the tail at 08:01:20 and 08:06:00, MMS detected very large fluctuations in the magnetic field with B_z ∼-25 nT. These strong pulses are of interest because they could be associated with the substorm trigger, as will be discussed next.

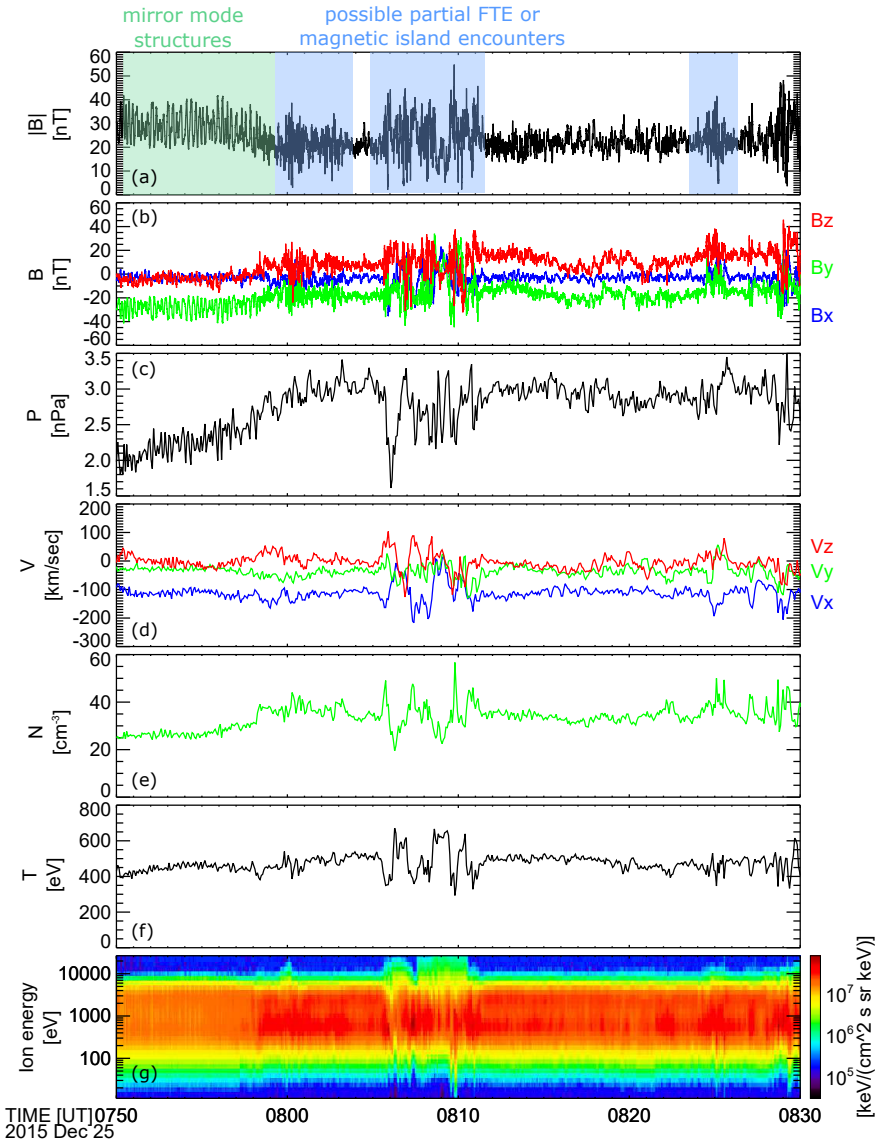

Figure 5. Magnetic field strength (a) and vectors (b), plasma pressure (c), velocity (d), density (e), temperature (f), and ion energy (g) in the magnetosheath observed by MMS1.

3.4. Timing Analysis and Substorm Trigger

The fortuitous near-alignment of several spacecraft missions along the Earth-Sun line during the 25 December 2015 event allows us to analyze the substorm time history on a global scale. Given the distances between observation points along the X-axis and flow speeds in each region, we can determine the propagation delays between events. The propagation speed of opened field lines from the dayside magnetopause to the tail is not constant. Rather, the lines travel more slowly until they reach the dawn-dusk terminator, then they accelerate to the solar wind speed in the tail. To determine a global timeline, we assume a flow speed in the magnetosheath of -100 km/sec, as was observed by MMS. Once the flow reaches the dawn-dusk terminator, it will have accelerated again to near the solar wind speed of -540 km/sec. Therefore, from the magnetopause to X = 0, we assume the flow speed to be the midpoint of the magnetosheath speed and the solar wind speed, -220 km/sec. Table 2

summarizes the flow speeds and resultant propagation delays for each region. Table 3 shows a time history of the global magnetosphere for the events leading up to the substorm onset.

It is generally accepted that the storage of energy in the magnetotail requires requires anti-parallel magnetic fields at the dayside magnetopause. This occurs most effectively for southward IMF. Using the previously determined propagation delay from Geotail to the inferred reconnection site of , a B_z component associated with dayside reconnection would be expected at the Geotail location 17.5 minutes prior to the tail reconnection, or approximately 07:56. However, the magnetic field observed by Geotail shows that B_z is positive after 07:51 and has only small negative values (∼-2 nT) from 07:40 to 07:51 UT. Thus, the expected strong negative B_z signature is not present. Though there was not a component at around 8:00 which would have could have triggered the substorm, persistent southward IMF and large solar wind flow speed was observed from 07:00 to 07:40. The high dynamic pressure acting upon the magnetosphere during this interval would have caused a large amount of magnetic flux to accumulate in the tail, thus driving the system to a state in which as substorm was imminent. The weakening negative or positive B_z component after 07:40 did not provide enough of a disturbance to actually trigger the substorm and the system remained in a marginally unstable state. We consider the localized but large-amplitude magnetic field fluctuations observed in the magnetosheath as a possible trigger mechanism for the substorm. As given in Table 2, the time delay from the MMS location to the reconnection site is approximately 12 minutes. This indicates that the signatures observed by MMS could be related to a system disturbance which would propagate tailward and arrive at the mid-tail reconnection site very close to the previously inferred time of ∼08:14, potentially triggering the substorm. In the minutes prior to 08:00, MMS observed large fluctuations in the magnetic field magnitude which were anticorrelated with fluctuations in the plasma pressure. These characteristics are indicative of a mirror mode instability [*Tsurutani et al.*, 1982; *Dimmock et al.*, 2015]. Mirror structures are non-propagating and predominantly occur in regions where the plasma $\beta < 5$, which is the case for this interval. The presence of a mirror mode instability in close proximity to the possible dayside reconnection site is significant because mirror modes structures could produce anomalous resistivity which may help initiate magnetic reconnection [*Treumann et al.*, 2004]. Mirror modes have recently been considered as closely related to transient reconnection at the magnetopause [*Laitinen et al.*, 2010]. The observed mirror mode instability could be an important phenomenon which initiated reconnection in the dayside, setting off a chain of events which eventually resulted in the substorm. We propose several possibilities regarding the fluctuations observed by MMS. (1) It is feasible that the pulsations are a smaller-scale structure in the solar wind which was not detected by the upstream monitors. When passing through the bow shock, the magnitudes increased by a typical shock compression factor of ∼4, thus explaining the large amplitudes. (2) The pulse could have formed as a result of a kinetic shock process due to a discontinuity in the solar wind hitting the bow shock. (3) This is a structure near the magnetopause boundary through which MMS momentarily passed, such as a flux transfer event (FTE) or magnetic island produced by dayside reconnection. FTEs occur when transient reconnection events in the magnetopause separate flux tubes from the magnetosphere which then propagate along the boundary [*Russell and Elphic*, 1978]. Though the parameters on either side of the pulses which were encountered from 08:00 to 08:11 are consistent with magnetosheath plasma, it is possible that MMS briefly entered the magnetopause boundary during this interval, as the spacecraft was in close proximity to the magnetopause location. Indeed, these bursts of strong B_z fluctuations are associated with simultaneous magnetosheath and magnetospheric-like energy population and positive v_z values. The plasma densities range from 20-30 cm^{-3} when the higher energy population is present. The colder component plasma in these fluctuations has even higher densities of 50-60 cm^{-3}. The relatively high densities could be associated with a cold plasmaspheric plume [e.g., *Elphic et al.*, 1996; *Goldstein et al.*, 2003], which has been shown to affect the dayside reconnection dynamics. This configuration, in which dense plasma from the plume reconnects with the magnetosheath plasma, is called asymmetric reconnection [*Cassak and Shay*, 2007]. Several studies [*Walsh et al.*, 2014a, b] have shown that when a plasmaspheric plume is present, the reconnection jets have lower velocities and larger densities. The higher densities decrease the reconnection rate, indicating a weakening of the solar wind-magnetosphere coupling. Finally, these large-scale MMS perturbations could be magnetic islands generated by turbulent reconnection in the magnetosheath [*Retinò et al.*, 2007; *Karimabadi et al.*, 2014]. A comprehensive analysis of these structures in beyond the scope of this paper, however, a deHoffman-Teller analysis was conducted and the results are provided in the Appendix.

4. Simulation Results

The global magnetosphere was modeled for the 25 December 2015 substorm using the SWMF/BATS-R-US model from NASA's Community Coordinated Modeling Center. A custom, high-resolution grid was generated with the region bounded by $-70 < x < 16, |y| < 24, |z| < 12$ resolved with a 1/4 R_E. A finer grid of 1/8 R_E resolution was added to the likely reconnection site locations: $-48 < x < 0, |y| < 24, |z| < 12$ R_E and a sphere around the Earth with a radius of 16 R_E. The

Table 2. Summary of locations, flow speeds, and time delays for timing analysis.

Initial Point	X_i [R_E]	Final Point	X_f [R_E]	Flow Speed [km/sec]	Time Delay [min]
Geotail	17.5	bow shock	15	540	1.3
bow shock	15	magnetopause	10.8	100	4.5
magnetopause	10.8	terminator	0	220	5.2
terminator	0	reconnection site	-33.2	540	6.5

Table 3. Timeline of events during the 25 December 2015 substorm.

Time [UT]	Location	Instrument	Event
07:51:10	solar wind	Geotail	IMF turns northward
08:01:00	magnetosheath	MMS	magnetic fluctuations
08:14:00	X_{GSM} = -33.2 R_E	-	inferred tail reconnection
08:17:05	far tail	P1	tailward flows increase
08:17:05	near tail	P3-P5	dipolarization signature
08:17:33	ground	GBOs	Pi2 pulsations
08:19:20	far tail	P2	tailward flows increase
08:19:50	far tail	P1	magnetic structures
08:20:10	far tail	P2	magnetic structures
08:33:00	far tail	P1,2	tailward flows cease

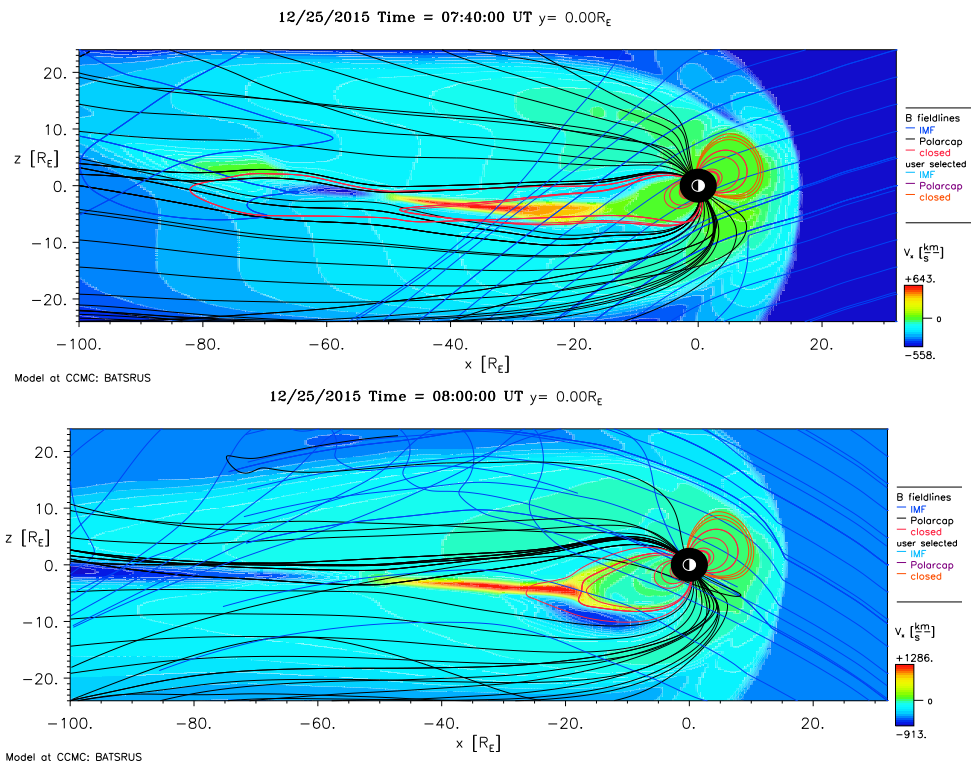

Figure 6. X-Z plane view of the global magnetosphere simulation results at 07:40 (upper) and 08:00 (lower). The black lines indicate open magnetic field lines, red lines indicate closed, and blue lines are the IMF. The color indicates the flow speed in the X-GSM direction. Red regions indicate earthward flow and blue regions indicate tailward flow.

model timestep is 1 minute. The actual Geotail data (shown in Figure 4) was used as an input to the model (propagated upstream to the model boundary at X = 33 R_E). The simulation results are shown in Figure 6. Strong earthward and tailward jets consistent with reconnection are visible as early as 07:40, indicating that the model produced reconnection earlier than observed. The X-line location remains between -55 and -50 R_E until 08:30, at which time it retreats beyond the simulation domain. The flows steadily increase from 07:40 to 08:00, reaching a maximum magnitude at 08:00 of approximately 1250 km/sec earthward and 1000 km/sec tailward. A plasmoid is ejected from the reconnection site tailward at 07:45. Figure 7 shows a comparison between data from THEMIS P3 and a virtual THEMIS P3 in the simulation. In the simulation results, the virtual P3 probe observes outflow jets with a maximum velocity near 600 km/sec and magnetic field structures, both of which correlate very well with the observations. The outflow observed by THEMIS P3 from 07:50 to 08:00 is not detected by THEMIS P4 or P5, which were separated by less than 0.3 R_E in X, less than 1 R_E in Z, and

shared the same Y coordinate. This indicates that the flow channel was spatially localized, corresponding to a bursty bulk flow (BBF) rather than a dipolarization front. BBFs are caused by spatially and temporally localized reconnection events and are the dominant mechanism for earthward mass, energy, and flux transfer in the midtail [*Angelopoulos et al.*, 1994; *Wiltberger et al.*, 2015]. The model produces these signatures 14 minutes earlier than they actually occurred, so the virtual probe data in Figure 7 has been shifted by 14 minutes. Once time-shifted, the simulation and observations agree very closely for both the BBF from 07:50 to 08:00 and the dipolarization signatures at 08:17. Though the BBF event indicates reconnection activity before 08:00, this does not suggest a substorm onset time earlier than previously determined. A number of other factors have been used to determine the later onset time of approximately 08:14 which are not present at this earlier time. The ARTEMIS field and plasma observations do not indicate a tailward moving plasmoid around 08:00. There are no Pi2 pulsations detected on the ground and there is minimal auroral activity at this time. Further, after the flows from 07:50 to 08:00, the magnetic field strength remains large (B_x = -45 nT) until the dipolarization at 08:17. These factors indicate that the signature observed by THEMIS P3 between 07:50 and 08:00 is indeed a localized BBF, rather than a global field reconfiguration consistent with a substorm. During the BBF, some of the flux accumulated in the tail during the long interval of solar wind driving from 07:15 to 07:40 was released into particle kinetic and thermal energy, though the energy transfer was not significant enough to trigger a substorm. As a result, the global magnetosphere remained in a marginally unstable state in which a large amount of energy was stored in the magnetotail. The weakening solar wind coupling after from 07:40 did not provide a sufficient trigger to cause substorm onset. BATS-R-US is an ideal MHD code which does not include a model for the small-scale physics associated with magnetic reconnection. Numerical diffusion associated with the discretized simulation grid manifests itself as increased resistivity in the plasma. Such resistivity is what violates the frozen-in condition and allows reconnection to occur. One interpretation of the numerical resistivity is that two magnetic field lines can reconnect if they meet in the same grid cell. Though a special, high-resolution grid was used in the areas where reconnection is likely to occur, the grid sizes remain much larger than the typical scale sizes of reconnection regions. One likely reason for the 14 minute time discrepancy in the simulation results is that the physical processes which cause reconnection take place over some time, whereas the simulation field lines can reconnect more readily and over a wider region because of the numerical resistivity, resulting in higher reconnection rate. Overall, the effects of numerical resistivity for this specific simulation have not been comprehensively analyzed.

5. Conclusion and Discussion

We have presented observations of the 25 December 2015 substorm and traced the flow of energy from the solar wind and dayside magnetosheath to the near-Earth magnetosphere, tail region at lunar orbit, and to the ground. We have shown evidence of the magnetosphere driven to a marginally unstable state by strong solar wind forcing which initiated a localized reconnection event, a burst bulk flow, observed by THEMIS P3. This may have relaxed some of the magnetic energy stored in the magnetotail. Subsequently as the solar wind forcing weakened, the magnetotail stayed in the marginally unstable state, until finally exploding into a plasmoid releasing substorm. Geotail data showed no apparent clear trigger that could initiate the substorm. The main conclusions are are as follows:

1. Timing analysis conducted on the ARTEMIS and THEMIS data reveals a reconnection site near 33 R_E and a reconnection time around 08:14. This is consistent with previous work which applied timing methods to measurements collected with much smaller probe separations. The onset time of Pi2 pulsations on the ground corroborates the determined substorm onset time and tail reconnection location.
2. The fortuitous near-alignment of several spacecraft missions along the Earth-Sun line during the 25 December 2015 substorm allows us to extend the timing analysis to the global scale, constructing a time history all the way from the solar wind during the growth phase to the energy dissipation of the expansion phase.
3. Global MHD simulations show a fair, qualitative agreement, with the model and observations differing by 14 minutes in the time at which reconnection occurred.
4. Solar wind observations before the onset time do not show the southward IMF condition typically associated with substorms. We conclude that persistent southward IMF approximately one hour before the substorm constitutes the substorm growth phase.
5. The pulsations observed by MMS are associated with the trigger that ultimately initiated the substorm onset. Further investigation of the detailed magnetosheath signatures is left for future studies.

Real-time forecasting of the arrival times of the complex solar wind structures at bow shock nose and their subsequent impact on the geo-space system is one of the most compelling problems of the space-weather research. Typically, data from a solar wind monitor at L1 is used as an input for global magnetospheric space weather models. For the event described here, the upstream data was conveniently available from Geotail spacecraft which located just upstream of the bowshock, which was used as an input for the global MHD code. While the qualitative agreement of the reconnection signatures between THEMIS and simulated data was excellent, the timing was 14 minutes off, suggesting

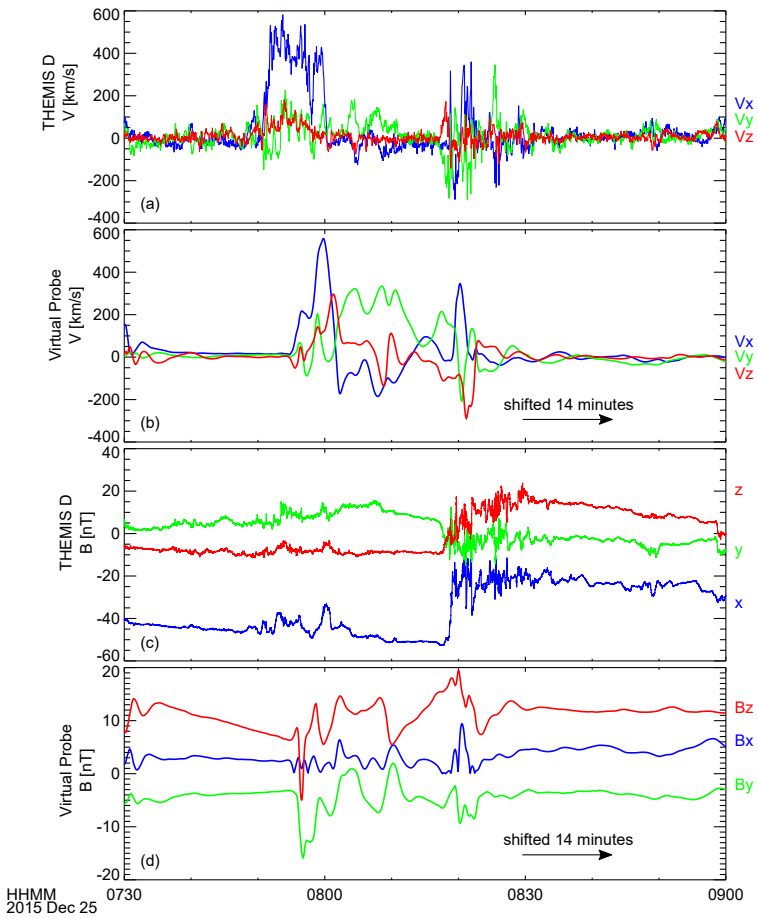

Figure 7. THEMIS P3 actual and virtual probe plasma velocity (a, b) and magnetic field (c, d) data. The virtual probe data has been time-shifted by 14 minutes to more clearly show the agreement between the model and observations.

that numerical resistivity of the global code may have initiated reconnection earlier in the simulation than in the real system. Our timing analysis indicated that large negative B_z-components observed by the MMS spacecraft in the magnetosheath could have been associated with the final trigger for the substorm initiation, and which was not present in the Geotail data. These observations and simulations suggest, that in order to achieve more accurate space weather forecasting, more solar wind monitors are needed covering perpendicular (with respect to solar wind flow) scale comparable to the size of the magnetosphere. Also, the numerical resistivity in global MHD models should further be improved and possibly include parameterized anomalous resistivity terms, to account for missing kinetic physics, such as mirror modes.

Acknowledgments. We acknowledge NASA contract NAS5-02099 and V. Angelopoulos for use of data from the THEMIS Mission. Specifically: D. Larson and R. P. Lin for use of SST data, C. W. Carlson and J. P. McFadden for use of ESA data, K. H. Glassmeier, U. Auster and W. Baumjohann for the use of FGM data provided under the lead of the Technical University of Braunschweig and with financial support through the German Ministry for Economy and Technology and the German Center for Aviation and Space (DLR) under contract 50 OC 0302, S. Mende and E. Donovan for use of the ASI data, the CSA for logistical support in fielding and data retrieval from the GBO stations, and NSF for support of GIMNAST through grant AGS-1004736, S. Mende and C. T. Russell for use of the GMAG data and NSF for support through grant AGS-1004814. Data provided by the Geophysical Institute Magnetometer Array operated by the Geophysical Institute, University of Alaska. More information about this dataset is available at http://magnet.asf.alaska.edu/. Geotail magnetic field and plasma data were provided by T. Nagai (H. Hayakawa and/or Y. Saito) through DARTS at Institute of Space and Astronautical Science, JAXA in Japan. Simulation results have been provided by the Community Coordinated Modeling Center at Goddard Space Flight Center through their public Runs on Request system (http://ccmc.gsfc.nasa.gov). The CCMC is a multi-agency partnership between NASA, AFMC, AFOSR, AFRL, AFWA, NOAA, NSF and ONR. The SWMF/BATSRUS Model was developed by the Center for Space Environment Modeling at the University of Michigan. We thank Maria Kuznetsova for creating the custom, high-resolution grid for the simulations.

References

Akasofu, S.-I. (1964), The development of the auroral substorm, *Planetary and Space Science*, *12*(4), 273–282.

Angelopoulos, V. (2008), The THEMIS mission, in *The THEMIS Mission*, vol. 141, pp. 5–34, Springer.

Angelopoulos, V. (2011), The ARTEMIS mission, *Space science reviews*, *165*(1-4), 3–25.

Angelopoulos, V., C. F. Kennel, F. V. Coroniti, R. Pellat, M. G. Kivelson, R. J. Walker, C. T. Russell, W. Baumjohann, W. C. Feldman, and J. T. Gosling (1994), Statistical characteristics

of bursty bulk flow events, *J. Geophys. Res.*, *99*, 21,257, doi: 10.1029/94JA01263.

Angelopoulos, V., J. P. McFadden, D. Larson, C. W. Carlson, S. B. Mende, H. Frey, T. Phan, D. G. Sibeck, K.-H. Glassmeier, U. Auster, et al. (2008), Tail reconnection triggering substorm onset, *Science*, *321*(5891), 931–935.

Atkinson, G. (1967), An approximate flow equation for geomagnetic flux tubes and its application to polar substorms, *Journal of Geophysical Research*, *72*(21), 5373–5382.

Auster, H., K. Glassmeier, W. Magnes, O. Aydogar, W. Baumjohann, D. Constantinescu, D. Fischer, K. Fornacon, E. Georgescu, P. Harvey, et al. (2009), The THEMIS fluxgate magnetometer, in *The THEMIS Mission*, pp. 235–264, Springer.

Axford, W. (1999), Reconnection, substorms and solar flares, *Physics and Chemistry of the Earth, Part C: Solar, Terrestrial & Planetary Science*, *24*(1), 147–151.

Baker, D., T. Pulkkinen, M. Hesse, and R. McPherron (1997), A quantitative assessment of energy storage and release in the earth's magnetotail, *Journal of geophysical research*, *102*, 7159–7168.

Baker, D. N., T. Pulkkinen, V. Angelopoulos, W. Baumjohann, and R. McPherron (1996), Neutral line model of substorms: Past results and present view, *Journal of Geophysical Research: Space Physics*, *101*(A6), 12,975–13,010.

Borovsky, J. E., R. J. Nemzek, and R. D. Belian (1993), The occurrence rate of magnetospheric-substorm onsets: Random and periodic substorms, *Journal of Geophysical Research: Space Physics*, *98*(A3), 3807–3813.

Caan, M. N., R. L. McPherron, and C. T. Russell (1977), Characteristics of the association between the interplanetary magnetic field and substorms, *Journal of Geophysical Research*, *82*(29), 4837–4842.

Cassak, P., and M. Shay (2007), Scaling of asymmetric magnetic reconnection: General theory and collisional simulations, *Physics of Plasmas*, *14*(10), 102,114.

Dimmock, A. P., A. Osmane, T. I. Pulkkinen, and K. Nykyri (2015), A statistical study of the dawn-dusk asymmetry of ion temperature anisotropy and mirror mode occurrence in the terrestrial dayside magnetosheath using themis data, *Journal of Geophysical Research: Space Physics*, pp. n/a–n/a, doi: 10.1002/2015JA021192, 2015JA021192.

Dungey, J. W. (1961), Interplanetary magnetic field and the auroral zones, *Physical Review Letters*, *6*(2), 47.

Elphic, R. C., L. A. Weiss, M. F. Thomsen, D. J. McComas, and M. B. Moldwin (1996), Evolution of plasmaspheric ions at geosynchronous orbit during times of high geomagnetic activity, *Geophysical Research Letters*, *23*(16), 2189–2192, doi: 10.1029/96GL02085.

Fu, H., Y. V. Khotyaintsev, A. Vaivads, M. André, and S. Huang (2012), Occurrence rate of earthward-propagating dipolarization fronts, *Geophysical Research Letters*, *39*(10).

Gabrielse, C., V. Angelopoulos, A. Runov, H. Frey, J. McFadden, D. Larson, K.-H. Glassmeier, S. Mende, C. Russell, S. Apatenkov, et al. (2009), Timing and localization of near-earth tail and ionospheric signatures during a substorm onset, *Journal of Geophysical Research: Space Physics*, *114*(A1).

Goldstein, J., B. R. Sandel, M. R. Hairston, and P. H. Reiff (2003), Control of plasmaspheric dynamics by both convection and sub-auroral polarization stream, *Geophysical Research Letters*, *30*(24), n/a–n/a, doi:10.1029/2003GL018390, 2243.

Ieda, A., S. Machida, T. Mukai, Y. Saito, T. Yamamoto, A. Nishida, T. Terasawa, and S. Kokubun (1998), Statistical analysis of the plasmoid evolution with Geotail observations, *Journal of Geophysical Research: Space Physics*, *103*(A3), 4453–4465.

Karimabadi, H., V. Roytershteyn, H. X. Vu, Y. A. Omelchenko, J. Scudder, W. Daughton, A. Dimmock, K. Nykyri, M. Wan, D. Sibeck, M. Tatineni, A. Majumdar, B. Loring, and B. Geveci (2014), The link between shocks, turbulence, and magnetic reconnection in collisionless plasmas, *Physics of Plasmas*, *21*(6), 062308, doi:10.1063/1.4882875.

Kokubun, S., T. Yamamoto, M. H. Acuña, K. Hayashi, K. Shiokawa, and H. Kawano (1994), The GEOTAIL magnetic field experiment, *Journal of geomagnetism and geoelectricity*, *46*(1), 7–22.

Laitinen, T., Y. V. Khotyaintsev, M. André, A. Vaivads, and H. Rème (2010), Local influence of magnetosheath plasma beta fluctuations on magnetopause reconnection, in *Annales Geophysicae*, vol. 28, p. 1053, Copernicus GmbH.

Liu, J., V. Angelopoulos, H. Frey, J. McFadden, D. Larson, K. Glassmeier, S. Mende, C. Russell, I. Rae, K. Murphy, et al. (2009), THEMIS observation of a substorm event on 04: 35, 22 february 2008, in *Annales Geophysicae*, vol. 27, pp. 1831–1841, Copernicus GmbH.

Liu, J., V. Angelopoulos, M. Kubyshkina, J. McFadden, K.-H. Glassmeier, and C. Russell (2011), Revised timing and onset location of two isolated substorms observed by time history of events and macroscale interactions during substorms (THEMIS), *Journal of Geophysical Research: Space Physics*, *116*(A5).

Lui, A. (1996), Current disruption in the earth's magnetosphere: Observations and models, *Journal of Geophysical Research: Space Physics*, *101*(A6), 13,067–13,088.

McFadden, J., C. Carlson, D. Larson, M. Ludlam, R. Abiad, B. Elliott, P. Turin, M. Marckwordt, and V. Angelopoulos (2008), The THEMIS esa plasma instrument and in-flight calibration, *Space Science Reviews*, *141*(1-4), 277–302.

McPherron, R. L., C. Russell, and M. Aubry (1973), Satellite studies of magnetospheric substorms on august 15, 1968: 9. phenomenological model for substorms, *Journal of Geophysical Research*, *78*(16), 3131–3149.

Mende, S., V. Angelopoulos, H. Frey, E. Donovan, B. Jackel, K.-H. Glassmeier, J. McFadden, D. Larson, and C. Carlson (2009), Timing and location of substorm onsets from THEMIS satellite and ground based observations, in *Annales Geophysicae*, vol. 27, pp. 2813–2830, Copernicus GmbH.

Moldwin, M. B., and W. J. Hughes (1992), On the formation and evolution of plasmoids: A survey of isee 3 Geotail data, *Journal of Geophysical Research: Space Physics*, *97*(A12), 19,259–19,282.

Mukai, T., S. Machida, Y. Saito, M. Hirahara, T. Terasawa, N. Kaya, T. Obara, M. Ejiri, and A. Nishida (1994), The low energy particle (lep) experiment onboard the Geotail satellite, *Journal of geomagnetism and geoelectricity*, *46*(8), 669–692.

Nagai, T., R. Nakamura, T. Mukai, T. Yamamoto, A. Nishida, and S. Kokubun (1997), Substorms, tail flows and plasmoids, *Advances in Space Research*, *20*(4-5), 961–971.

Nishida, A. (1983), Imf control of the earth's magnetosphere, *Space Science Reviews*, *34*(2), 185–200.

Øieroset, M., T. D. Phan, R. P. Lin, and B. U. Sonnerup (2000), Walén and variance analyses of high-speed flows observed by wind in the midtail plasma sheet: Evidence for reconnection, *Journal of Geophysical Research: Space Physics*, *105*(A11), 25,247–25,263.

Oka, M., T.-D. Phan, J. Eastwood, V. Angelopoulos, N. Murphy, M. Øieroset, Y. Miyashita, M. Fujimoto, J. McFadden, and D. Larson (2011), Magnetic reconnection x-line retreat associated with dipolarization of the earth's magnetosphere, *Geophysical Research Letters*, *38*(20).

Pollock, C., T. Moore, A. Jacques, J. Burch, U. Gliese, Y. Saito, T. Omoto, L. Avanov, A. Barrie, V. Coffey, et al. (2016), Fast plasma investigation for magnetospheric multiscale, *Space Science Reviews*, *199*(1-4), 331–406.

Pu, Z., X. Chu, X. Cao, V. Mishin, V. Angelopoulos, J. Wang, Y. Wei, Q. Zong, S. Fu, L. Xie, et al. (2010), THEMIS observations of substorms on 26 february 2008 initiated by magnetotail reconnection, *Journal of Geophysical Research: Space Physics*, *115*(A2).

Retinò, A., D. Sundkvist, A. Vaivads, F. Mozer, M. André, and C. J. Owen (2007), In situ evidence of magnetic reconnection in turbulent plasma, *Nature Physics*, *3*, 236–238, doi: 10.1038/nphys574.

Richardson, I., and S. Cowley (1985), Plasmoid-associated energetic ion bursts in the deep geomagnetic tail: Properties of the boundary layer, *Journal of Geophysical Research: Space Physics*, *90*(A12), 12,133–12,158.

Rostoker, G., S.-I. Akasofu, J. Foster, R. Greenwald, Y. Kamide, K. Kawasaki, A. Lui, R. McPherron, and C. Russell (1980), Magnetospheric substormsdefinition and signatures, *Journal of Geophysical Research: Space Physics*, *85*(A4), 1663–1668.

Runov, A., V. Angelopoulos, M. Sitnov, V. Sergeev, J. Bonnell, J. McFadden, D. Larson, K.-H. Glassmeier, and U. Auster (2009), THEMIS observations of an earthward-propagating dipolarization front, *Geophysical Research Letters*, *36*(14).

Runov, A., V. Angelopoulos, X.-Z. Zhou, X.-J. Zhang, S. Li, F. Plaschke, and J. Bonnell (2011), A THEMIS multicase study of dipolarization fronts in the magnetotail plasma sheet, *Journal of Geophysical Research: Space Physics*, *116*(A5).

Russell, C., B. Anderson, W. Baumjohann, K. Bromund, D. Dearborn, D. Fischer, G. Le, H. Leinweber, D. Leneman, W. Magnes, et al. (2014), The magnetospheric multiscale magnetometers, *Space Science Reviews*, *199*(1-4), 189–256.

Russell, C. T., and R. C. Elphic (1978), Initial ISEE magnetometer results: Magnetopause observations, *22*, 681–715, doi: 10.1007/BF00212619.

Saito, T. (1969), Geomagnetic pulsations, *Space Science Reviews*, *10*(3), 319–412.

Sergeev, V., R. Elphic, F. Mozer, A. Saint-Marc, and J. Sauvaud (1992), A two-satellite study of nightside flux transfer events in the plasma sheet, *Planetary and space science*, *40*(11), 1551–1572.

Slavin, J., E. Smith, B. Tsurutani, D. Sibeck, H. Singer, D. Baker, J. Gosling, E. Hones, and F. Scarf (1984), Substorm associated traveling compression regions in the distant tail: ISEE-3 Geotail observations, *Geophysical research letters*, *11*(7), 657–660.

Sonnerup, B., G. Paschmann, and T.-D. Phan (1995), Fluid aspects of reconnection at the magnetopause: In situ observations, *Physics of the Magnetopause*, pp. 167–180.

Torbert, R., C. Russell, W. Magnes, R. Ergun, P.-A. Lindqvist, O. LeContel, H. Vaith, J. Macri, S. Myers, D. Rau, et al. (2016), The fields instrument suite on MMS: Scientific objectives, measurements, and data products, *Space Science Reviews*, *199*(1-4), 105–135.

Tóth, G., I. V. Sokolov, T. I. Gombosi, D. R. Chesney, C. R. Clauer, D. L. De Zeeuw, K. C. Hansen, K. J. Kane, W. B. Manchester, R. C. Oehmke, et al. (2005), Space weather modeling framework: A new tool for the space science community, *Journal of Geophysical Research: Space Physics*, *110*(A12).

Tóth, G., B. Van der Holst, I. V. Sokolov, D. L. De Zeeuw, T. I. Gombosi, F. Fang, W. B. Manchester, X. Meng, D. Najib, K. G. Powell, et al. (2012), Adaptive numerical algorithms in space weather modeling, *Journal of Computational Physics*, *231*(3), 870–903.

Treumann, R., C. Jaroschek, O. Constantinescu, R. Nakamura, O. Pokhotelov, and E. Georgescu (2004), The strange physics of low frequency mirror mode turbulence in the high temperature plasma of the magnetosheath, *Nonlinear Processes in Geophysics*, *11*(5/6), 647–657.

Tsurutani, B., E. Smith, R. Anderson, K. Ogilvie, J. Scudder, D. Baker, and S. Bame (1982), Lion roars and nonoscillatory drift mirror waves in the magnetosheath, *Journal of Geophysical Research: Space Physics*, *87*(A8), 6060–6072.

Tsyganenko, N. (1989), A magnetospheric magnetic field model with a warped tail current sheet, *Planetary and Space Science*, *37*(1), 5–20.

Walsh, B., T. Phan, D. Sibeck, and V. Souza (2014a), The plasmaspheric plume and magnetopause reconnection, *Geophysical Research Letters*, *41*(2), 223–228.

Walsh, B., J. Foster, P. Erickson, and D. Sibeck (2014b), Simultaneous ground-and space-based observations of the plasmaspheric plume and reconnection, *Science*, *343*(6175), 1122–1125.

Wiltberger, M., V. Merkin, J. G. Lyon, and S. Ohtani (2015), High-resolution global magnetohydrodynamic simulation of bursty bulk flows, *Journal of Geophysical Research (Space Physics)*, *120*, 4555–4566, doi:10.1002/2015JA021080.

6. Appendix

6.1. Ground-Based Observations

During the substorm event on 25 December 2015, the ground-based magnetometer stations and all-sky imager observatories captured magnetic signatures and auroral intensification related to the magnetotail phenomena. Figure 9 shows data from the stations (arranged east to west) at Gillam, MB (GILL, magnetic latitude 66.00N, magnetic longitude 333.19W), Fort Smith, NT (FSMI, mag. 67.29N, 307.05W), Fort Simpson, NT (FSIM, mag. 67.23N, 294.41W), Petersburg, AK (PTRS, mag. 59.90N, 283.97W), Whitehorse, YT (WHIT, mag. 63.64N, 279.62W), Inuvik, NT (INUV, mag. 71.21N, 275.77W), and Poker Flat, AK (POKR, mag. 65.40N, 265.79W). In addition, the auroral electrojet (AE) index derived from the THEMIS magnetometer network is shown along with total intensity counts from the FSMI ASI. The location of each station and the ionospheric footprints of P3-P5 (traced using the Tsyganenko 89 model) are shown in Figure 8. Note that P1 and P2 were located at field lines which do not map to the Earth. At each of the stations, magnetic pulsations in the Pi2 range (40-150 sec) [*Saito*, 1969] associated with a substorm current wedge (SCW) are detected beginning at 08:17:33 (denoted by the dashed vertical line). Further, the AE index first decreases slightly then increases to ∼450 nT and the auroral intensity captured by the FMSI ASI increases sharply at this time. This is in agreement with the previously determined reconnection time, considering a typical time delay between reconnection and ground onset of 2-4 minutes.

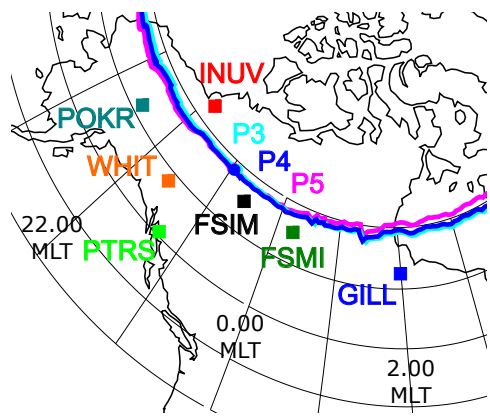

Figure 8. Locations of the ground-based observatories and footprints of the THEMIS probes at 08:17:00 traced using the Tsyganenko 89 model.

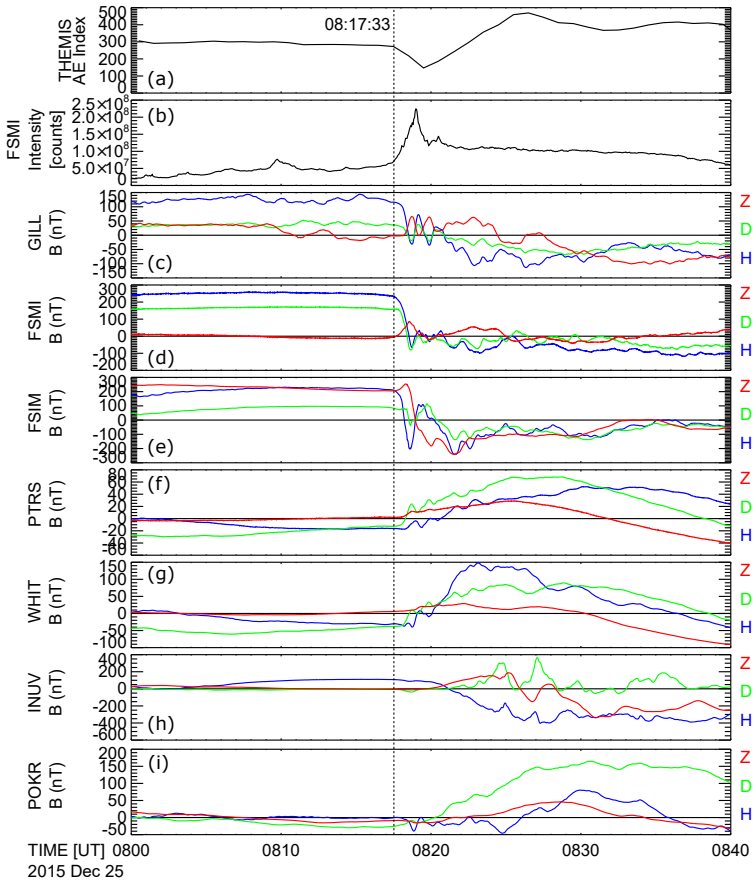

Figure 9. (a) THEMIS AE index, (b) total all-sky imager intensity at FSMI, and (c)-(j) ground based magnetometer data from stations arranged from east to west. The dashed vertical line indicates 08:17:33, the ground onset time of the substorm.

At FSIM and all stations eastward (GILL, FSMI), the initial turning of the D component is negative, whereas for PTRS and all stations westward (WHIT, INUV, POKR), the initial turning is positive. This indicates that the center of the SCW is located between FSIM and PTRS, corresponding closely to the THEMIS footprints and a magnetic local time of 23.00.

6.2. deHoffman-Teller Analysis of MMS Observations

To clarify what the structures observed by MMS are, deHoffman-Teller (HT) analysis has been conducted for all four MMS to find a deHoffman-Teller frame. The HT frame is a frame in which the electric field in the plasma goes to zero, indicating the passage of a quasi-static structure [*Sonnerup et al.*, 1995]. We find that such a frame exists for each MMS spacecraft using the

Table 4. HT Frame and Correlation of E with E_{HT} for each MMS Probe for 08:00:00 to 08:00:30

MMS	V_{HT} [km/sec]	Slope	Coeff.
1	[-145, -88, -0.9]	0.999	0.996
2	[-144, -84, 4.7]	1.00	0.998
3	[-143, -71, 10.2]	1.00	0.991
4	[-141, -68, 6.8]	1.00	0.994

Table 5. Walén Relation Test Results for Varying Time Windows

	Time Windows [Seconds after 08:00:00]					
	00 - 30		00 - 20		05 - 25	
MMS	Slope	Coeff.	Slope	Coeff.	Slope	Coeff.
1	-0.2	0.6	-0.1	0.3	-0.2	0.6
2	-0.2	0.7	-0.2	0.8	-0.2	0.7
3	-0.2	0.6	-0.4	0.8	-0.3	0.7
4	-0.2	0.5	-0.4	0.7	-0.2	0.5

time interval from 08:00:00 to 08:00:30. The determined velocity of the HT frame, V_{HT}, is given for each spacecraft, along with the slope and coefficient of $E = V \times B$ versus $E_{HT} = V_{HT} \times B$, are given in Table 4 and an example plot is given in Figure 10. As shown, the slope and correlation are near one in each case, indicating that the time variation observed is due to a steady structure moving past the probes at a velocity of V_{HT}. The large X and Y components of V_{HT} indicate that the structure is flowing tailward with the magnetosheath plasma which has been redirected around either side of the magnetopause. We also compute the Walén relation for each probe with varying time windows, as shown in Table 5. Note that the HT frame exists and the E versus E_{HT} slope and coefficient are near unity in each time window for which the Walén relation was computed. If the Walén relation is satisfied, it indicates that the plasma flow is Alfvénic in the HT frame, as is the case for rotational discontinuities associated with reconnection. In this case, the Walén relation is not well satisfied, suggested the plasma flow is not Alfvénic in the HT frame. Because the Walén relation is not satisfied, it is possible that MMS observes fossil FTEs or flux ropes produced by magnetosheath or dayside reconnection which previously operated, and which are then convected tailward with the magnetosheath flow. Unfortunately, burst mode satellite data is not available during this interval, so fast survey data is used in the analysis.

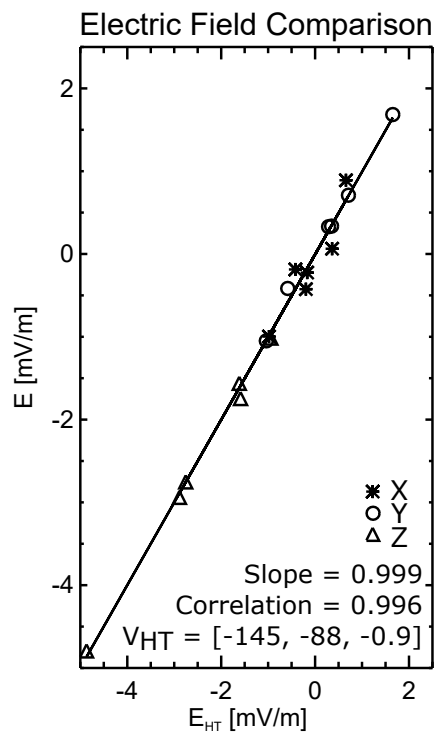

Figure 10. Example scatter plot for HT frame for MMS1 during the 08:00:00 to 08:00:30 interval. This plot is representative of those for MMS2-4.